Journal of ELECTRONIC MATERIALS, Vol. 50, No. 4, 2021
https://doi.org/10.1007/s11664-020-08286-5

ASIAN CONSORTIUM ACCMS–INTERNATIONAL CONFERENCE ICMG 2020

A Numerical Fitting-Based Compact Model: An Effective Way to Extract Solar Cell Parameters

SABYASACHI MUKHOPADHYAY ,[1,4] SEERAM RAMAKRISHNA,[2] AVISHEK KUMAR,[3] and GOUTAM KUMAR DALAPATI[1,2,5]

1.—Department of Physics, SRM University AP, Amaravati, Andhra Pradesh 522503, India. 2.—Center for Nanofibers and Nanotechnology, Faculty of Engineering, National University of Singapore, Singapore 117576, Singapore. 3.—Sunkonnect Pte. Ltd., 1 Cleantech Loop, Singapore 637141, Singapore. 4.—e-mail: sabyasachi.m@srmap.edu.in. 5.—e-mail: goutam.d@srmap.edu.in

We have developed an electrical circuit-based compact numerical fitting model to determine industry-related physical parameters of solar cells utilizing only 3–8 current–voltage coordinate points without any specific selection of an experimental coordinate axis. The proposed compact numerical fitting model was effectively tested to determine the peak power point, fill factor and efficiencies for organic and inorganic solar cells, as well as for solar panels. This research facilitates cost-effective energy management of solar modules and farms.

Key words: Compact model, solar cell, Thiele technique, series resistance

INTRODUCTION

Solar cells are one of the most promising devices for meeting rising demands of clean electric power generation.[1–8] To predict the performance of solar cells accurately, it is essential to have a precise set of solar cell parameters.[1–3,7–12] The lumped circuit models are the most commonly used method for describing the electrical characteristics of a solar cell and extracting the physical parameters from experimental data. Among the existing circuit models, the single exponential model (Fig. 1) is the simplest and most widely used method to describe the characteristics of a large variety of solar cells.[13–18] In the single exponential model (SEM), the current (I) and voltage (V) relation has an implicit form and is given by the following equation:[12]

$$I = I_{\mathrm{ph}} - I_0\left\{\exp\left(\frac{V + R_{\mathrm{s}}I}{nV_{\mathrm{th}}}\right) - 1\right\} - \frac{V + R_{\mathrm{s}}I}{R_{\mathrm{sh}}} \quad (1)$$

where I_{ph} is the photocurrent, I_0 represents the saturation current, V_{th} is a product of the Boltzmann constant, with temperature revived by electron charge q, n is the ideality factor, R_{s} is the series resistance and R_{sh} is the shunt resistance. An accurate estimation of these parameters is very important to provide precise evaluation of the performance of a solar cell.[10,11] Various methods have been developed to determine these parameters of solar cells.[1–3,8,9,11–13,16–18] The transcendental nature of the SEM increases the complexity of determination of solar cell parameters. As a result, the SEM has been expressed in explicit form using the Lambert function to avoid the complexity.[13–15] However, to determine the accurate set of parameters, many terms of the series are required to be computed and it increases complexity of the simulation. The physics-based compact models aid designers in creating advanced designs and more simply predict the performance of the new devices without need of complex simulation. Compact solar cell models are ideal for predicting the design parameters of solar cells from I–V characteristics without rigorous simulation. Compact modeling of a solar cell is the crucial step for shortening of the design cycle, which is necessary in today's

(Received March 27, 2020; accepted June 15, 2020; published online June 26, 2020)

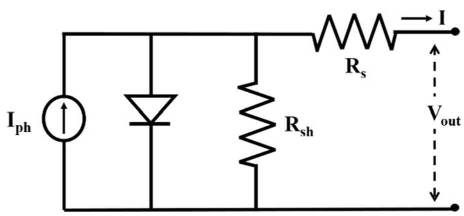

Fig. 1. Generic solar cell equivalent circuit with the single exponential model

competitive industry, and will be particularly helpful to device designers.

However, only a few works have attempted to introduce a compact model[7,12] for solar cell parameter extractions. Recently, based on the empirical model reported in Saleem and Karmalkar[7] and Karmalkar and Saleem,[8] Saleem et al.[7] presented empirical compact expressions for the solar cell parameters. However, the accuracy of their predicted results is sensitive to the selection of measured points. One of the useful compact models for determining the physical parameters of solar cells is that of Phang et al.[12] In their model, they have assumed R_{sh} is much bigger than the R_s (R_{sh} + R_s R_{sh}). Hence, parameters estimated (following Phang et al.[12]) for solar cells having high series resistance ($R_s \approx R_{sh}$), especially inorganic thin films, organic and hybrid photovoltaics, were inaccurate. The series resistance of a solar cell is a parasitic and dominant factor that affects conversion efficiency and current–voltage characteristics under illuminated condition. The energy loss resulting from the series resistance has risen because of the increase in the finger length and handling of large current. Therefore, accurate determination of series resistance becomes more important to obtain reliable characterization and optimization of cell designs to minimize such losses.[19–25] In the present article, we have developed a compact numerical fitting formula for determining solar cell parameters, based on the single exponential model. Our compact model aims to focus on the improvement of the predicted series resistance from field data.

The maximum power point and fill factor of a solar cell are also important parameters for designing high-efficiency solar cells.[8,9] The current–voltage relation of a solar cell has an implicit form and requires iterative calculation to determine these parameters. There are many methods in the literature for determining these parameters, including empirical models[8,9] to the curve-fitting technique.[2,10,11] Generally, the polynomial interpolations are used to estimate the maximum power point and fill factor. However, the polynomial technique requires rich experimental I–V data with smooth variation of applied bias to estimate the accurate parameters. Increasing the number of measured points inherently increases the effect of noise. In the present article, we have employed the Thiele interpolation technique based on the curve fitting to determine the peak power point and fill factor from few measured points (3–6) of the current–voltage characteristic. It is shown that the Thiele interpolation method can accurately estimate the maximum power point and fill factor with fewer measurement points in the current–voltage characteristic.

THEORETICAL BACKGROUND

Equation 1 is an implicit equation and it is not possible to solve it analytically. However, using the Lambert W function, the solution for current and voltage ($V = V_{out}$) can be expressed as

$$V = I_{ph}R_{sh} + I_0R_{sh} - I(R_s + R_{sh}) - nV_{th}W\left\{\frac{I_0R_{sh}}{nV_{th}}\exp\left(\frac{I_{ph}R_{sh} + I_0R_{sh} - IR_{sh}}{nV_{th}}\right)\right\} \quad (2)$$

where W represents the Lambert W function.

The short-circuit current I_{sc}, by substituting V = 0 and $I = I_{sc}$ in Eq. 2, and open-circuit voltage V_{oc}, by substituting $V = V_{oc}$, I = 0 in Eq. 2, can be given by

$$I_{sc} = -\frac{1}{R_s}W\left(\frac{R_sI_0R_{sh}\exp\left(\frac{R_{sh}(R_sI_{ph}+R_sI_0)}{nV_{th}(R_s+R_{sh})}\right)}{nV_{th}(R_s+R_{sh})}\right) + \frac{R_{sh}(I_{ph}+I_0)}{R_s+R_{sh}} \quad (3a)$$

and

$$V_{oc} = I_{ph}R_{sh} - nV_{th}W\left(\frac{I_0R_{sh}\exp\left(\frac{R_{sh}(I_{ph}+I_0)}{nV_{th}}\right)}{nV_{th}}\right) + I_0R_{sh} \quad (3b)$$

Using Eqs. 3a and 3b, the photocurrent I_{ph} and saturation current I_0 can be given by

$$I_0 = \frac{(I_{sc}(R_s+R_{sh}) - V_{oc})\exp\left(-\frac{V_{oc}}{nV_{th}}\right)}{R_{sh}\left(1 - \left(\exp\left(-\frac{V_{oc}-R_sI_{sc}}{nV_{th}}\right)\right)\right)} \quad (4a)$$

and

$$I_{ph} = \frac{V_{oc}}{R_{sh}} + \left(\exp\left(\frac{V_{oc}}{nV_{th}}\right) - 1\right)\frac{(I_{sc}(R_s+R_{sh}) - V_{oc})\exp\left(-\frac{V_{oc}}{nV_{th}}\right)}{R_{sh}\left(1 - \exp\left(-\frac{V_{oc}-R_sI_{sc}}{nV_{th}}\right)\right)} \quad (4b)$$

By substituting Eqs. 4a and 4b in Eq. 2 and making the assumption of $\Delta \equiv \exp\{-(V_{oc} -$

$R_sI_{sc})/nV_{th}\} \ll 1$, which is generally valid for a large variety of solar cells,[10,11] Eq. 2 is simplified to

$$V = I_{sc}(R_s + R_{sh}) - I(R_s + R_{sh}) - nV_{th}W\left(\frac{(I_{sc}(R_s + R_{sh}) - V_{oc})}{nV_{th}}\exp\left(-\frac{V_{oc}}{nV_{th}}\right)\exp\left(\frac{I_{sc}(R_s + R_{sh}) - IR_{sh}}{nV_{th}}\right)\right) \tag{5}$$

Using the reverse of the Lambert function, the current and voltage relation can be expressed as

$$V = (I_{sc} - I)(R_s + R_{sh}) - (I_{sc}(R_s + R_{sh}) - V_{oc})\exp\left(\frac{V - V_{oc} + IR_s}{nV_{th}}\right) \tag{6}$$

From Eq. 6, the derivative of V with respect to I can be given by:

$$\frac{dV}{dI} = \frac{-(R_s + R_{sh}) + \frac{R_s}{nV_{th}}(V - (I_{sc} - I)(R_s + R_{sh}))}{1 - \frac{V - (I_{sc} - I)(R_s + R_{sh})}{nV_{th}}} \tag{7}$$

The short-circuit dynamic resistance R_{sho}, by substituting $V = 0$ and $I = I_{sc}$ in Eq. 7, and open-circuit dynamic resistance R_{so}, by substituting $V = V_{oc}$, I = 0 in Eq. 7, can be given by

$$\left.\frac{dV}{dI}\right|_{V=0} = -R_{sho} = -(R_s + R_{sh}) \tag{8a}$$

and

$$\left.\frac{dV}{dI}\right|_{I=0} = -R_{so} = \frac{-(R_s + R_{sh}) + \frac{R_s}{nV_{th}}(V_{oc} - I_{sc}(R_s + R_{sh}))}{1 - \frac{V_{oc} - I_{sc}(R_s + R_{sh})}{nV_{th}}} \tag{8b}$$

For a maximum power $\partial(I \cdot V)/\partial I = 0$, so that Eq. 7 becomes

$$\left.\frac{dV}{dI}\right|_{V=V_m,\, I=I_m} = -\frac{V_m}{I_m} = -\frac{-(R_s + R_{sh}) + \frac{R_s}{nV_{th}}(V_m - (I_{sc} - I_m)(R_s + R_{sh}))}{1 - \frac{V_m - (I_{sc} - I_m)(R_s + R_{sh})}{nV_{th}}} \tag{9}$$

where I_m represents the maximum power current and V_m represents the maximum power voltage. By

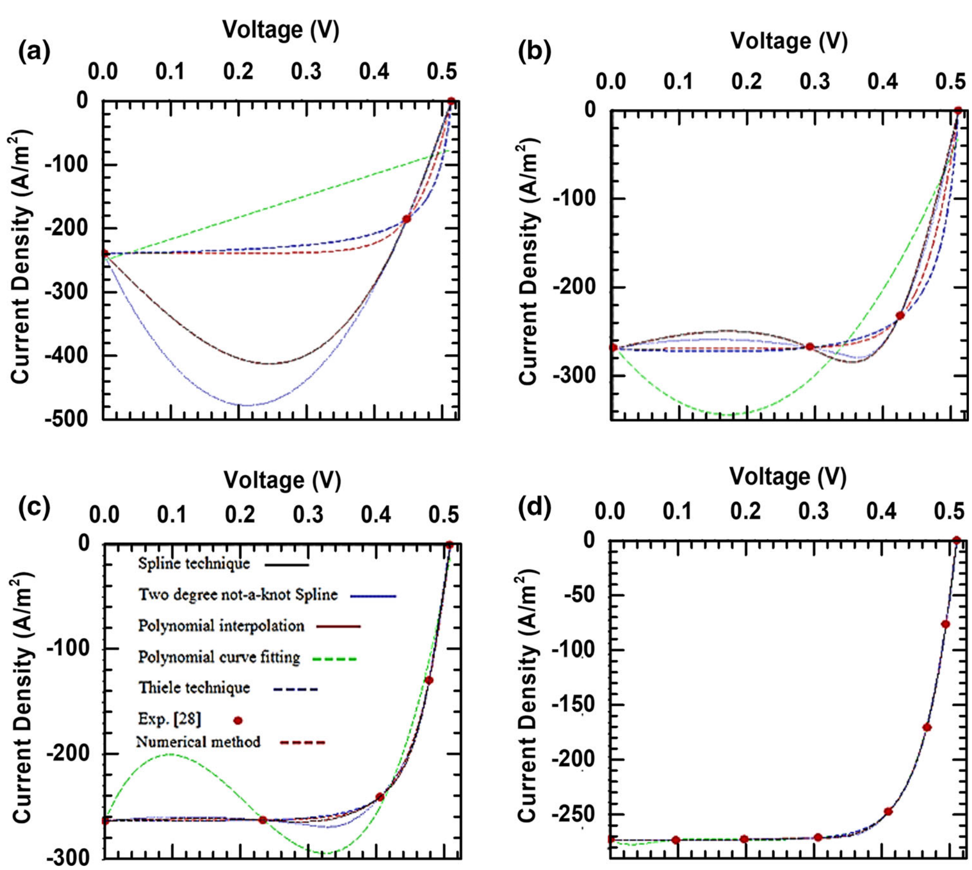

Fig. 2. Comparison of rebuilt I–V curves of a silicon solar cell at T = 50°C for (a) three measurements, (b) four measurements, (c) five measurements and (d) eight measurements of the bias point.

Table I. Estimated maximum power point (V_m, I_m or J_m) and fill factor (FF) by spline technique (ST), two-degree spline technique (TDST), polynomial interpolation (PI), polynomial curve fitting (PCF) and Thiele technique (TT) for three and four measurements of the bias point of a silicon solar cell at T = 50°C, and the results obtained by an exact numerical method

Number of measured points	Three points					Four points					
Method	ST	TDST	PI	PCF	TT	ST	TDST	PI	PCF	TT	Numerical value
V_m (V)	0.35	0.33	0.33	0.37	0.43	0.40	0.40	0.39	0.33	0.43	0.42
J_m (Am^{-2})	−399.3	−446.6	−446.6	−137.5	−217.9	−266.5	−263.7	−265.8	−270.8	−231.4	−239.9
FF	1.02	1.08	1.08	0.37	0.68	0.77	0.76	0.76	0.65	0.72	0.72
DP of FF (%)	40.2	49.4	49.4	48.5	5.7	5.9	5.1	5.1	9.4	0.7	0

Table II. Estimated maximum power point (V_m, I_m or J_m) and fill factor (FF) by the spline technique (ST), two-degree spline technique (TDST), polynomial interpolation (PI), polynomial curve fitting (PCF) and Thiele technique (TT) for five and eight measurements of the bias point of a silicon solar cell at T = 50°C, and the results obtained by exact numerical method

Number of measured points	Five points					Eight points					
Method	ST	TDST	PI	PCF	TT	ST	TDST	PI	PCF	TT	Numerical value
V_m (V)	0.42	0.40	0.42	0.39	0.42	0.41	0.41	0.42	0.42	0.42	0.42
J_m (Am^{-2})	−236.5	−248.6	−236.6	−275.7	−237.1	−240.8	−243.8	−239.0	−240.2	−239.8	−239.9
FF	0.73	0.73	0.73	0.78	0.73	0.72	0.72	0.72	0.72	0.72	0.72
DP of FF (%)	0.16	0.35	0.35	7.02	0.13	0.013	0.07	0.013	0.05	0	0

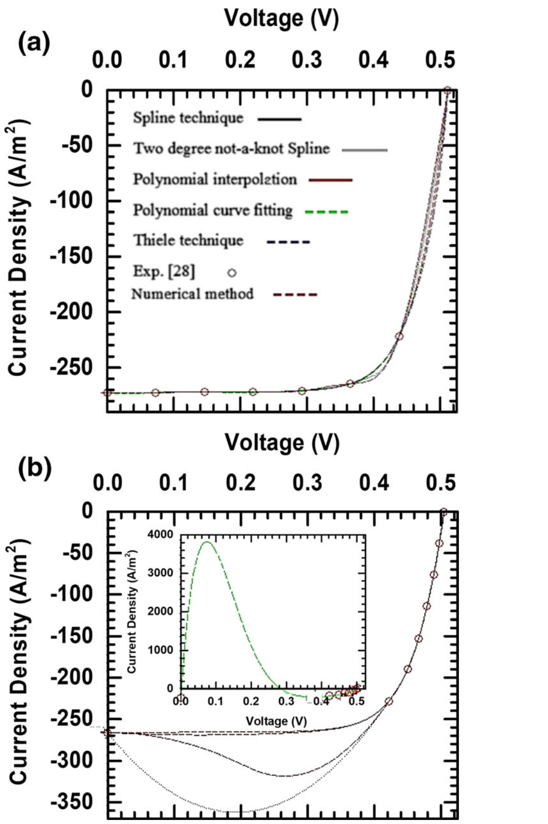

Fig. 3. Comparison of rebuilt I–V curves of a silicon solar cell at T = 50°C for eight selected points with (a) equal space on the V axis and (b) equal space on the I axis. The deviation of the model with insignificant data is shown in 3b (inset).

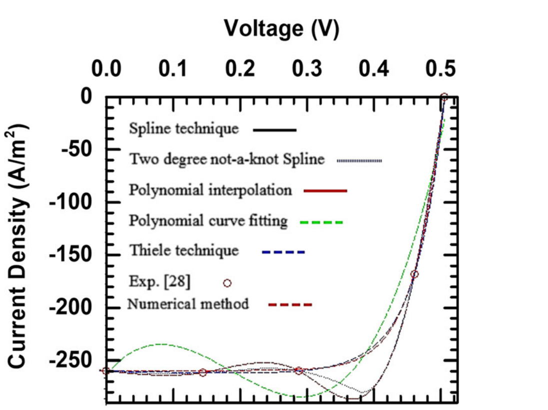

Fig. 4. Comparison of rebuilt I–V curves of a silicon solar cell at T = 50°C after adding random noise to the measured points.

substituting Eq. 8a into Eqs. 8b and 9, we have obtained the following relations for the R_{so} and maximum power:

$$R_{\mathrm{so}} = -\frac{-R_{\mathrm{sho}} + \frac{R_{\mathrm{s}}}{nV_{\mathrm{th}}}(V_{\mathrm{oc}} - I_{\mathrm{sc}}R_{\mathrm{sho}})}{1 - \frac{V_{\mathrm{oc}} - I_{\mathrm{sc}}R_{\mathrm{sho}}}{nV_{\mathrm{th}}}} \tag{10}$$

and

$$\frac{V_{\mathrm{m}}}{I_{\mathrm{m}}} = \left(-R_{\mathrm{sho}} + \frac{R_{\mathrm{s}}}{nV_{\mathrm{th}}}(V_{\mathrm{m}} - (I_{\mathrm{sc}} - I_{\mathrm{m}})R_{\mathrm{sho}})\right) / \left(1 - \frac{V_{\mathrm{m}} - (I_{\mathrm{sc}} - I_{\mathrm{m}})R_{\mathrm{sho}}}{nV_{\mathrm{th}}}\right) \tag{11}$$

Equation (10) can be written as

$$n = \left(\frac{R_{\mathrm{so}} - R_{\mathrm{s}}}{R_{\mathrm{sho}} - R_{\mathrm{so}}}\right)\left(\frac{I_{\mathrm{sc}}R_{\mathrm{sho}} - V_{\mathrm{oc}}}{V_{\mathrm{th}}}\right) \tag{12}$$

The closed form expression for n in the terms of measured parameters can be represented by substituting Eq. 12 in Eq. 11, as

$$n = \frac{\beta}{\alpha V_{\mathrm{th}}} \tag{13a}$$

where

$$\beta = -V_{\mathrm{m}}R_{\mathrm{sho}}(I_{\mathrm{sc}} - I_{\mathrm{m}}) + V_{\mathrm{m}}^2 + I_{\mathrm{m}}(R_{\mathrm{sho}}(I_{\mathrm{sc}} - I_{\mathrm{m}}) - V_{\mathrm{m}})R_{\mathrm{so}} \tag{13b}$$

$$\alpha = V_{\mathrm{m}} - R_{\mathrm{sho}}I_{\mathrm{m}} - \frac{I_{\mathrm{m}}(R_{\mathrm{sho}}(I_{\mathrm{sc}} - I_{\mathrm{m}}) - V_{\mathrm{m}})(R_{\mathrm{so}} - R_{\mathrm{sho}})}{R_{\mathrm{sho}}I_{\mathrm{sc}} - V_{\mathrm{oc}}} \tag{13c}$$

Substituting Eq. 13a in Eq. 10, the R_{s} can be given by

$$R_s = \frac{(R_{so} - R_{sho})\beta + \alpha R_{so}(R_{sho}I_{sc} - V_{oc})}{(R_{sho}I_{sc} - V_{oc})\alpha} \tag{14}$$

Substituting Eq. (14) in Eq. (8a), the R_{sh} can be given by

$$R_{\mathrm{sh}} = R_{\mathrm{sho}} - \frac{(R_{\mathrm{so}} - R_{\mathrm{sho}})\beta + \alpha R_{\mathrm{so}}(R_{\mathrm{sho}}I_{\mathrm{sc}} - V_{\mathrm{oc}})}{(R_{\mathrm{sho}}I_{\mathrm{sc}} - V_{\mathrm{oc}})\alpha} \tag{15}$$

Substituting Eqs. 13, 14 and 15 in Eqs. 4a and 4b, the I_0 and I_{ph} can be given by

$$I_0 = \left(I_{\mathrm{sc}} + \frac{R_{\mathrm{s}}I_{\mathrm{sc}} - V_{\mathrm{oc}}}{R_{\mathrm{sh}}}\right)\exp\left(-\frac{\alpha V_{\mathrm{oc}}}{\beta}\right) \tag{16}$$

and

$$I_{\mathrm{ph}} = I_{\mathrm{sc}} - \left(I_{\mathrm{sc}} + \frac{R_{\mathrm{s}}I_{\mathrm{sc}} - V_{\mathrm{oc}}}{R_{\mathrm{sh}}}\right)\exp\left(-\frac{\alpha V_{\mathrm{oc}}}{\beta}\right) + \frac{R_{\mathrm{s}}I_{\mathrm{sc}}}{R_{\mathrm{sh}}} \tag{17}$$

Equations. 13, 14, 15, 16 and 17 can be used to determine corresponding values of n, R_{s}, R_{sh}, I_0 and I_{ph} from measured parameters.

Table III. Estimated maximum power point (V_m, I_m or J_m) and fill factor (FF) by the spline technique, two-degree spline technique, polynomial interpolation, polynomial curve fitting and the Thiele technique for five bias points with random noise of a silicon solar cell at T = 50°C, and the results obtained by an exact numerical method

Number of measured points	Five points					
Method	ST	TDST	PI	PCF	TT	Numerical value
V_m (V)	0.41	0.41	0.41	0.38	0.42	0.42
J_m (Am^{-2})	280.08	−277.11	−266.27	−263.03	−237.1	−239.91
FF	0.84	0.83	0.79	0.72	0.72	0.72
DP from ideal value of V_m (%)	1.42	0.71	1.47	9.09	0.038	0
DP from ideal value of J_m (%)	16.7	15.5	11.0%	9.6%	1.2%	0
DP of FF (%)	15.07	14.69	9.45	0.33	1.20	0

RESULTS AND DISCUSSION

The accuracy of the presented Eqs. 13, 14, 15, 16 and 17 for determining the parameters of solar cells depends on the accuracy of measurements of I_m, V_m, R_{so} and R_{sho}. The values of I_m, V_m, R_{so} and R_{sho} can be determined from the measured current–voltage coordinates (I, V) utilizing curve-fitting techniques. The high-degree polynomial curve-fitting technique is employed to estimate these parameters.[10,11] But the technique requires very smooth experimental data to reduce the errors that originate from the Runge effect.[12] Furthermore, many factors may influence the measured current-voltage coordinates and introduce noise to the measured I–V data. In addition, fluctuations in the measured current–voltage coordinates reduce smoothness of experimental data and causes a large numerical error in the estimated parameters as obtained from the polynomial method. To resolve these problems, Chan et al.[26] discussed a subsection polynomial curve-fitting technique. In this method, the experimental current–voltage curve is divided into several subsections and for each subsection, low-degree polynomial curve fitting is used. Although the method can estimate the parameters precisely, it requires a large number of points. The accuracy of the estimated parameters is greatly influenced by the position of the selected subsections and experimental points. By employing the Thiele curve-fitting technique, we have solved the aforementioned problems even with a lower number of measured I–V coordinates. The developed method is less dependent on the position of the selected experimental I–V coordinates.

The I_m and V_m were extracted from the measured I–V coordinates by using the spline technique (ST), two-degree not-a-knot spline technique (TDST), polynomial interpolation (PI), polynomial curve fitting (PCF) and the Thiele technique (TT).

In Fig. 2, we have compared the predicted I–V curve using the spline technique, two-degree not-a-knot spline technique, polynomial interpolation, polynomial curve fitting and Thiele technique for 3, 4, 5 and 8 I–V coordinate points of a silicon solar cell at a measurement temperature of 50°C. For comparison, we have also plotted the ideal I–V curve obtained by Chan et al.[26] As shown in this figure, the rebuilt I–V curve using the Thiele interpolation technique is very close to the ideal one while using fewer measured I–V coordinates. The estimated maximum power points, using the aforementioned techniques, are tabulated in Tables I and II. The deviation percentage (DP) is also presented in the tables. The DP is a factor which differentiates between a compact model and a numerical model for parameter extraction. As shown in Tables I and II, the estimated maximum power points using the Thiele technique are more accurate than the other methods.

Being realistic, we also simulate I–V curves from eight measurements of the bias point with different spacing utilizing the spline technique, two degree not-a-knot spline technique, polynomial interpolation, polynomial curve fitting and the Thiele technique, as depicted in Fig. 3. Selected I–V coordinates have the equal space on the V axis for Fig. 3a, while for Fig. 3b, selected points have equal space on the I axis. The deviation in the fitting model with insignificant data points is shown in the inset of Fig. 3b. As demonstrated in this figure, the polynomial and spline method is more sensitive to the position of selected points. To further investigate the sensitivity of our employed approach to the fluctuations in the measured data or noise, the data incorporated with the random noise has been analyzed with our employed technique to estimate the maximum power point and fill factor. As illustrated in Fig. 4, the fitted curve using the Thiele curve-fitting technique is in very good agreement with the ideal numerical method one.

Also, as shown in Table III, the estimated maximum power point using the Thiele technique is very accurate even for the data with random noise. In the rest of the article, we have employed our Thiele curve-fitting technique to estimate precisely the values of I_m, V_m, R_{so} and R_{sho} from an experimentally measured current–voltage curve.

Table IV. Predicted parameters by our model and Phang et al.[12] and extracted parameters by Zhang et al.[10] of a multi-junction small-molecule cell under different illumination at T = 27°C

	58 mW/cm^2 (27°C)					116 mW/cm^2 (27°C)					372 mW/cm^2 (27°C)				
Parameters	This work	Zhang et al.	Phang et al.	DP (%) this work	DP (%) Phang et al.	This work	Zhang et al.	Phang et al.	DP (%) this work	DP (%) Phang et al. (%)	This work	Zhang et al.	Phang et al.	DP (%) this work	DP (%) Phang et al.
R_s (Ω cm^2)	50.3	50.9	43.5	1	14.50	47.0	46.9	42.02	0.35	10.4	23.1	23.1	21.66	0.21	6.2
R_{sh} (kΩ cm^2)	2.9	2.9	3.01	0.77	0.91	1.4	1.4	1.4	0.37	3.2	0.409	0.41	0.4329	0.50	5.09
I_{ph} (mA)	2.3	2.3	2.3	0.35	0.44	4.7	4.7	4.7	0.014	0.33	0.018	0.015	0.0185	20.7	20.7
I_0 ($\times 10^{-3}$ mA)	2.05	1.7	2.53	21.10	49.40	1.2	1.04	1.9	15.3	83.4	0.61	0.4	0.13	49.7	67.6
n	6.3	6.3	6.5	0.03	3.46	5.8	5.8	6.2	0.58	5.90	5.12	5.16	5.578	0.761	8.05
I_{sc} (mA/cm^2)	−2.27	−2.2	–	0.17	–	−4.5	−4.5	–	0.003	–	−17.4	−17.5	–	0.057	–
V_{oc} (V)	1.12	1.12	–	0.02	–	1.22	1.2	–	0.08	–	1.34	1.34	–	0.0014	–

Table V. Predicted parameters by our model and Phang et al.[12] and extracted parameters by Zhang et al.[10] of a silicon cell at T = 33°C, a silicon solar module at T = 45°C and a DSSC at T = 20°C

	Silicon solar cell (33°C)					Silicon solar module (45°C)					DSSC (20°C)				
Parameters	This work	Zhang et al.	Phang et al.	DP (%) this work	DP (%) Phang et al.	This work	Zhang et al.	Phang et al.	DP (%) this work	DP (%) Phang et al.	This work	Zhang et al.	Phang et al.	DP (%) this work	DP (%) Phang et al.
R_s (Ω)	0.037	0.03	0.037	0.268	0.321	1.31	1.31	1.30	0.01	0.7	44.5	44.7	42. 50	0.4	4.9
R_{sh} (kΩ)	0.04	0.04	0.04	0	0	0.60	0.60	0.60	0.2	0.003	3.3	3.28	3.3	1.03	2.4
I (A)	0.76	0.76	0.76	0.004	0.004	1.03	1.03	1.033	0.005	0.006	0.002	0.002	0.002	0.04	0.09
I_0 (μA)	0.23	0.24	0.23	1.696	4.128	1.59	1.59	1.67	0.12	4.6	0.014	0.015	0.02	6.8	44
n	1.45	1.45	1.45	0.207	0.4189	45.81	45.8	45.9	0.09	0.27	2.37	2.38	2.46	0.67	3.2
I_{sc} (A)	−0.76	−0.76	–	0.00013	–	−1.03	−1.03	–	0.0009	–	−0.002	−0.002	–	0	–
V_{oc} (V)	0.57	0.57	–	0	–	16.78	16.7	–	0.0005	–	0.70	0.7	–	0.01	–

Table VI. Predicted parameters by our model and Phang et al.[12] and extracted parameters by Zhang et al.[10] of a P3HT stand-alone polymer solar cell, PCPDTBT stand-alone polymer solar cell and tandem solar cell at $T = 27°C$

P3HT cell (27°C)						PCPDTBT cell (27°C)					Tandem cell (27°C)				
Parameters	This work	Zhang et al.	Phang et al.	DP (%) this work	DP (%) Phang et al.	This work	Zhang et al.	Phang et al.	DP (%) this work	DP (%) Phang et al.	This work	Saetre et al[27]	Chen et al.[28]	DP (%) This work	DP (%) Gao et al.[2]
R_s (Ω cm^2)	1.2	1.2	1.16	0.8	3.2	5.40	5.4	4.46	0.018	17.2	5.6	5.6	5.42	0.66	3.09
R_{sh} (kΩ cm^2)	0.64	0.68	0.68	0.16	0.33	0.17	0.17	0.18	0.094	3.1	1.23	1.2	1.24	0	0.45
I_{ph} (mA)	10.8	10.8	10.8	0.38	0.39	9.49	9.4	9.44	0.07	0.5	7.82	7.82	7.82	0.0025	0.016
I_0															

($\times 10^{-7}$ mA)383440.711.416.22.63.84.930.630.98.98.89.61.518.6n1.651.651.650.030.361.741.741.820.0174.73.023.023.0300.0060.46I_{sc} (mA cm^{-2})–10.8–10.8–0––9.2–9.22–0––7.79–7.79–0.00012–V_{oc} (V)0.60.63–0.015–0.660.66–0–1.23991.24–0.008–

To investigate the reliability of our presented compact numerical fitting model, the physical parameters of a large variety of solar cells were predicted and compared with the other numerical results in the following. Our presented compact model is used to predict the parameters of silicon solar cells (at $T = 33°C$), a silicon solar module (at $T = 45°C$), DSSC (20°C), P3HT cell (27°C), PCPDTBT cell (27°C), tandem cell (27°C) and a multi-junction small-molecule cell under different illumination. The estimated I_m, V_m, R_{so} and R_{sho} for these solar cells and the parameters predicted by our compact model are tabulated in Tables IV, V and VI. Also, our results have been compared with the results obtained by the numerical method[10] and the compact model presented in Phang et al.[12] As shown in Tables V and VI, our predicted results are very close to the numerical results, and the DP of the parameters predicted by our method are better than the reported results by Phang et al.[12] and Chan et al.[26] The DP of the parameters predicted by our method is less than 1% except for saturation current. It could be because of the approximation employed in our method.

It is well recognized that series and shunt resistance (R_s) values significantly influence the solar cell performance, and highly accurate prediction of such low values of series resistance is very important.[25,27–37] Our predicted results for R_s are almost the same as the numerical results, and the DP of our predicted results for this parameter is much better than that obtained by Phang et al.,[12] especially for non-silicon solar cells and for multi-junction small-molecule cells (Tables VII and VIII).

CONCLUSION

In this article, we have explored a new compact numerical fitting model, focusing on improvement of predicted series resistance. The circuit equations are directly derived from a single exponential model and are useful for determining the physical parameters of solar cells more easily. With three to eight current–voltage points from random experimental coordinates, as obtained from different crystalline to non-crystalline photovoltaic cells, we established that our compact numerical fitting model, could predict physical parameters with high accuracy. In addition, it was demonstrated that Thiele interpolation appears to be more accurate for predicting the maximum power point and fill factor with fewer measurements of the bias point even in the presence of random noise. The implementation of our compact numerical fitting model will help to obtain in-field load matching parameters to enrich energy management techniques for small-scale solar modules to large-scale solar farms.

Table VII. Details of parameters estimated by the Thiele technique used to predict parameters of a multi-junction small-molecule cell under different illumination, tandem and stand-alone polymer solar cells

	Stand-alone polymer and tandem cells			Multi-junction small-molecule cell under different illumination		
Type of solar cell	P3HT cell (27°C)	PCPDTBT cell (27°C)	Tandem cell (27°C)	58 mW/cm^2 (27°C)	116 mW/cm^2 (27°C)	372 mW/cm^2 (27°C)
R_{so} (Ω m^2)	0.00054	0.00128	0.00170	0.013	0.00850	0.00316
R_{sho} (Ω m^2)	0.0685	0.0185	0.1241	0.301	0.144	0.0432
V_m (V)	0.5079	0.499	0.9942	0.7650	0.801	0.825
J_m (A/m^2)	−93.21	−61.87	−65.2336	−16.73	−33.561	−128.46

Table VIII. Details of parameters estimated by the Thiele technique used to predict parameters of a silicon solar cell, a silicon solar cell module and a DSSC

Type of solar cell	Silicon solar cell (33°C)	Silicon solar module (45°C)	DSSC (20°C)
R_{so} (Ω)	0.0884	2.5608	76.2198
R_{sho} (V)	42.081	602.33	3364.158
V_m (V)	0.4521	12.656	0.5013
I_m (A)	−0.688	−0.91214	−0.00169

ACKNOWLEDGMENTS

SM and GKD thank SRM University, AP research funding for financial support. SM acknowledge SERB- DST, Govt. of India for Early Career Research Award Grants (ECR/2017/001937). SR acknowledges the support provided by NUS Hybrid-Integrated Flexible (Stretchable) Electronic Systems (HiFES) Program Seed Fund (grant no. R265000628133).

REFERENCES

1. F. Yu, G. Huang, W. Lin, and C. Xu, *IEEE Trans. Electron Devices* 66, 670 (2019).
2. X. Gao, Y. Cui, J. Hu, G. Xu, Z. Wang, J. Qu, and H. Wang, *Energy Convers. Manag.* 157, 460 (2018).
3. F. Yu, G. Huang, and C. Xu, *Renew. Energy* 146, 2188 (2020).
4. V.J. Chin and Z. Salam, *Appl. Energy* 237, 519 (2019).
5. S.P. Aly, S. Ahzi, and N. Barth, *Appl. Energy* 236, 728 (2019).
6. X. Sun, T. Silverman, R. Garris, C. Deline, and M.A. Alam, *IEEE J. Photovolt.* 6, 1298 (2016).
7. H. Saleem and S. Karmalkar, *IEEE Electron Device Lett.* 30, 349 (2009).
8. S. Karmalkar and H. Saleem, *IEEE Electron Device Lett.* 29, 449 (2008).
9. S. Karmalkar and H. Saleem, *Sol. Energy Mater. Sol. Cells* 95, 1076 (2011).
10. C. Zhang, J. Zhang, Y. Hao, Z. Lin, and C. Zhu, *J. Appl. Phys.* 110, 064504 (2011).
11. K. Ishibashi, Y. Kimura, and M. Niwano, *J. Appl. Phys.* 103, 094507 (2008).
12. J.C.H. Phang, D.S.H. Chan, and J.R. Phillips, *Electron. Lett.* 20, 406 (1984).
13. A. Jain and A. Kapoor, *Sol. Energy Mater. Sol. Cells* 81, 269 (2004).
14. X. Gao, Y. Cui, J. Hu, N. Tahir, and G. Xu, *Energy Convers. Manag.* 171, 1822 (2018).
15. A. Jain, S. Sharma, and A. Kapoor, *Sol. Energy Mater. Sol. Cells* 90, 25 (2006).
16. J. Ding and R. Radhakrishnan, *Sol. Energy Mater. Sol. Cells* 92, 1566 (2008).
17. W. Kim and W. Choi, *Sol. Energy* 84, 1008 (2010).
18. F. Khan, S.N. Singh, and M. Husain, *Sol. Energy* 85, 2288 (2011).
19. F. Ghani and M. Duke, *Sol. Energy* 85, 2386 (2011).
20. P. Singh, M. Lal, and S.N. Singh, *Sol. Energy Mater. Sol. Cells* 91, 137 (2007).
21. M.-K. Lee, J.-C. Wang, S.-F. Horng, and H.-F. Meng, *Sol. Energy Mater. Sol. Cells* 94, 578 (2010).
22. J. Hyung Lee, Y. Hyun Lee, J. Yong Ahn, and J.-W. Jeong, in *19th International Photovoltaic Science and Engineering Conference and Exhibition. PVSEC-19 Jeju Korea 9–13 November, 2009*, vol. 95 (2011), p. 22.
23. J. Lauwaert, K. Decock, S. Khelifi, and M. Burgelman, *Sol. Energy Mater. Sol. Cells* 94, 966 (2010).
24. C. Chibbaro, M. Zimbone, G. Litrico, P. Baeri, M.L. Lo Trovato, and F. Aleo, *J. Appl. Phys.* 110, 044505 (2011).
25. W. Liu, L. Hu, S. Dai, L. Guo, N. Jiang, and D. Kou, *Electrochim. Acta* 55, 2338 (2010).
26. D.S.H. Chan, J.R. Phillips, and J.C.H. Phang, *Solid-State Electron.* 29, 329 (1986).
27. T.O. Saetre, O.-M. Midtgård, and G.H. Yordanov, *Renew. Energy* 36, 2171 (2011).
28. Y. Chen, X. Wang, D. Li, R. Hong, and H. Shen, *Appl. Energy* 88, 2239 (2011).
29. D. Tan, C.T. Chua, G.K. Dalapati, and D. Chi, *Thin Solid Films* 520, 2336 (2012).
30. G.K. Dalapati, S.L. Liew, A.S.W. Wong, Y. Chai, S.Y. Chiam, and D.Z. Chi, *Appl. Phys. Lett.* 98, 013507 (2011).
31. S.L. Liew, Y. Chai, H.R. Tan, H.K. Hui, A.S.W. Wong, G.K. Dalapati, and D.Z. Chi, *J. Electrochem. Soc.* 159, H52 (2011).
32. A. Ortiz-Conde, F.J. García Sánchez, and J. Muci, *Sol. Energy Mater. Sol. Cells* 90, 352 (2006).
33. H. Bayhan and M. Bayhan, *Sol. Energy* 85, 769 (2011).
34. S. Masudy-Panah, S. Zhuk, H.R. Tan, X. Gong, and G.K. Dalapati, *Nano Energy* 46, 158 (2018).
35. S. Zhuk, A. Kushwaha, T.K.S. Wong, S. Masudy-Panah, A. Smirnov, and G.K. Dalapati, *Sol. Energy Mater. Sol. Cells* 171, 239 (2017).
36. G.K. Dalapati, S. Masudy-Panah, A. Kumar, C. Cheh Tan, H. Ru Tan, and D. Chi, *Sci. Rep.* 5, 17810 (2015).

37. S. Zhuk, T.K.S. Wong, S.S. Hadke, S. Lie, A. Guchhait, Y. Gao, L.H. Wong, S. Cheng, X. Wang, and G.K. Dalapati, *Sol. Energy* 194, 777 (2019).